IL NUOVO CIMENTO Vol. 110 B, N. 2 Febbraio 1995

A novel method to detect quantum states of the radiation field

G. M. D'Ariano ([1])([2]), Chiara Macchiavello([1]), Matteo G. A. Paris([1])

([1]) *Dipartimento di Fisica "Alessandro Volta", via A. Bassi 6, I-27100 Pavia, Italy*
([2]) *INFN Sezione di Pavia via A. Bassi 6, I-27100 Pavia, Italy*

(ricevuto 18 Ottobre 1994; approvato 22 Novembre 1994)

Summary. — We propose a new method for detecting the density matrix of the radiation field via optical homodyne tomography. The tomographic reconstruction is greatly improved, with very fast data analysis and very reliable statistics on-line with detection. The Wigner function of the input field is reconstructed also for quantum superpositions of states. We analyze the sensitivity of Quantum Tomography in detecting the photon number, the field quadratures, and the phase of radiation field. A comparison between results of Quantum Tomography and direct detection of these quantities (photodetection, single homodyne detection, and double homodyne detection respectively), is given at fixed energy impinged into the experimental apparatus. We show that, despite tomographic reconstruction provides a complete characterization of the field state, it is more noisy than single-observable detection schemes.

1. – Introduction

In the quantum description of radiation all knowable properties of the field are contained in the density matrix and, in principle, an experimental detection of the quantum state is equivalent to detect the probability distribution of any desired observable. Recently, Smithey et al.[1] have experimentally demonstrated the possibility of detecting the density matrix by means of repeated measurements of the field-quadrature $\hat{a}_\phi = \frac{1}{2}(ae^{-i\phi} + a^\dagger e^{i\phi})$ at various phases ϕ's. The symmetrized Wigner function $W(\alpha, \bar{\alpha})$ is recovered from the distribution of the homodyne outcomes $p(x, \phi)$ through the "tomographic" formula[2]

$$W(\alpha,\bar{\alpha}) = \frac{1}{4}\int_{-\infty}^{\infty} d\eta\,|\eta| \int_{-\infty}^{\infty} dx \int_0^{\pi} \frac{d\phi}{\pi}\, p(x,\phi) \exp\left\{ i\eta \left[x - Re\left(\alpha e^{i\phi}\right)\right]\right\}\,, \tag{1}$$

and the reconstruction of $W(\alpha, \bar{\alpha})$ from a finite-numerable set of homodyne outcomes is actually achieved by means of a filtered inverse Radon transform, similarly to the original technique of X-ray or NMR tomography (for this reason the method has been

called "Quantum Tomography"). The density matrix in the configuration representation is obtained through the Fourier transform

$$\langle x+x'|\hat{\rho}|x-x'\rangle = \int_{-\infty}^{\infty} dy\, e^{2ix'y} W(x+iy, x-iy)\ , \tag{2}$$

whereas the number representation is achieved by means of the further integration steps

$$\begin{aligned} \langle n|\hat{\rho}|m\rangle \equiv \rho_{n,m} &= \frac{1}{\sqrt{\pi 2^n 2^m n! m!}} \\ &\int_{-\infty}^{\infty} dx \int_{-\infty}^{\infty} dx' e^{-\frac{1}{2}(x^2+x'^2)} H_n(x) H_m(x')\ \langle x|\hat{\rho}|x'\rangle\ , \end{aligned} \tag{3}$$

where $H_n(x)$ is the Hermite polynomial of degree n. The point of this method is the Filtered inverse Radon transform, a smoothing procedure on experimental data which is equivalent to an *a priori* assumption on the detected density matrix. This introduces systematic errors on any reconstructed quantity, prevents from evaluating reliable statistical errors, and makes the method affected by fast quantum oscillations of the Wigner function itself.

Very recently we have proposed an alternative method that completely overcomes the above difficulties.[3] The novel method relies on the same experimental setup (see Fig. 1), but uses a different algorithm for reconstructing the density matrix. The algorithm needs no assumption on the state, and is unaffected by oscillations of the Wigner function, because the density matrix is recovered directly from averages on data. The resulting tomographic reconstruction is extremely faster than the original filtered technique, and provides very reliable statistics on-line with detection. In Sect. 2 we briefly describe

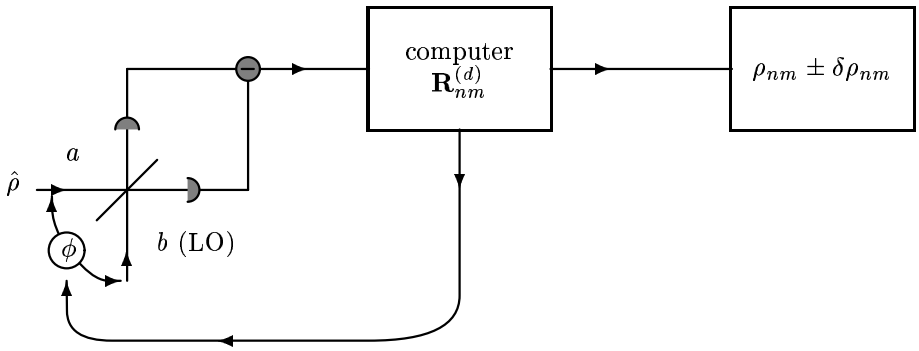

Fig. 1. – Scheme of homodyne tomographic detection

the reconstruction algorithm. In Sect. 3 we show how to obtain the Wigner function from the detected state. Finally in Sect. 4 we analyze the sensitivity of the tomographic reconstruction, and compare it with the sensitivity achieved by conventional detection of single-observables. We show that, despite tomographic reconstruction provides a complete characterization of the field state, it is not convenient when only one quantity is of interest.

2. – Description of the method

The density matrix elements $\rho_{n,m}$ in the number representation can be obtained by the Husimi Q-function $Q(\alpha,\bar{\alpha})$ through the formula

$$\rho_{n,m} = \frac{1}{\sqrt{n!m!}} \frac{\partial^n}{\partial \bar{\alpha}^n} \frac{\partial^m}{\partial \alpha^m} \left(Q(\alpha,\bar{\alpha})\, \mathrm{e}^{|\alpha|^2} \right) \Big|_{\alpha=\bar{\alpha}=0} . \tag{4}$$

The function $Q(\alpha,\bar{\alpha})$ is related to the experimental homodyne probabilities as follows[2]

$$Q(\alpha,\bar{\alpha}) = \frac{1}{4\pi} \int_{-\infty}^{\infty} d\eta\, |\eta| \int_{-\infty}^{\infty} dx \int_0^{\pi} d\phi\, p(x,\phi) \exp\left\{ -\frac{1}{8}\eta^2 + i\eta \left[x - Re\left(\alpha e^{i\phi}\right) \right] \right\} . \tag{5}$$

After evaluating derivatives in Eq. (4) analytically, Eqs. (5) and (4) connect the matrix elements $\rho_{n,m}$ to simple averages on homodyne data. Let us denote by $\bar{\rho}_{n,m}$ the experimental mean value of $\rho_{n,m}$ obtained from Eqs. (5) and (4) when integral over x and ϕ are replaced with the corresponding experimental averages. Typically the average on the phase ϕ is evaluated by summing over F equally spaced values $\phi_f = \frac{f\pi}{F}$ $(f = 0, ..., F-1)$. A lengthy but straightforward derivation leads to the following reconstruction formula

$$\bar{\rho}_{n,n+d} = \sum_{m=0}^{[n+\frac{1}{2}d]} \frac{1}{F} \sum_{f=0}^{F-1} \mathbf{R}^{(d)}_{nm}(\phi_f) \left\langle \mathbf{H}^{(d)}_{nm}(x) \right\rangle_{\phi_f} , \tag{6}$$

where $d \geq 0$, the brackets $\langle ... \rangle_{\phi_f}$ denote averaging over the subensemble of data for fixed phase $\phi = \phi_f$ (with experimental outcome x), $[z]$ is the integer part of z, and the averaged function $\mathbf{H}^{(d)}_{nm}(x)$ is given by

$$\mathbf{H}^{(d)}_{nm}(x) = e^{-2x^2} x^{\langle d \rangle_2} \Phi\left(m - n - \frac{1}{2}d - \frac{1}{2}\langle d+1 \rangle_2, \frac{1}{2} + \langle d \rangle_2; 2x^2 \right) . \tag{7}$$

In Eq. (7) the notation $\langle z \rangle_2$ denotes the rest of the division $z/2$, whereas $\Phi(\alpha,\beta;z)$ is the confluent hypergeometric function of z with parameters α, β.[4] The fixed matrix $\mathbf{R}^{(d)}_{nm}(\phi)$ in Eq. (6) is given by

$$\begin{aligned} \mathbf{R}^{(d)}_{nm}(\phi) = {} & \left(2^{3/2} i\right)^{\langle d \rangle_2} \frac{2^{n+\frac{d}{2}+1}}{\sqrt{n!(n+d)!}} (-i)^{2n+d} \\ & \times \sum_{j_1=0}^{n} \sum_{j_2=0}^{d} (-1)^{j_2} \binom{n}{j_1} \binom{d}{j_2} (2n+d-2j_1-j_2)!(2j_1+j_2)! \\ & \times \sum_{l_1=0}^{n-j_1+[\frac{d-j_2}{2}]} \sum_{l_2=0}^{j_1+[\frac{j_2}{2}]} \frac{(-8)^{-l_1-l_2} (\cos\phi)^{2n+d-2j_1-j_2-2l_1} (\sin\phi)^{2j_1+j_2-2l_2}}{l_1! l_2! (2j_1+j_2-2l_2)! (2n+d-2j_1-j_2-2l_1)!} \\ & \times \Gamma\left(n + \frac{1}{2}d - l_1 - l_2 + \frac{1}{2}\langle d \rangle_2 + 1 \right) \delta_{m,l_1+l_2} . \end{aligned} \tag{8}$$

Despite apparent complexity of Eqs. (6-8) the average in Eq. (6) is particularly suited to on-line data analysis. In fact, apart from the sum over data, the procedure requires just a single sum over m, whereas the hypergeometric functions $\Phi(\alpha,\beta;z)$ are connected each other iteratively, and the matrix $\mathbf{R}^{(d)}_{nm}(\phi_f)$ is stored in the machine before beginning experiments.

We have tested our method on some Monte Carlo simulated experiments, with the aim of evaluating both the correctness of error statistics and the absence of any systematic deviation from theoretical values. In order to evaluate the statistical errors, we have preliminarily studied the distribution of the tomographic outcomes for each matrix element around its averaged value, checking that it is perfectly Gaussian for every matrix element, independently on the kind of considered quantum state (we have considered coherent, squeezed, and general quantum superpositions of number states). Then, relying on normal distribution of deviations $\delta\rho_{n,m}$, the error $\varepsilon_{n,m}$ of the matrix element $\rho_{n,m}$ has been evaluated as usual, namely by dividing the ensemble of data into subensembles (here also called 'experiments'), and then calculating the r.m.s. deviation of the subensemble average with respect to the global average. A sample histogram for the first 30×30 matrix elements is given in Fig. 2, for a coherent state with $\langle n\rangle = 4$. Notice that about 68% of deviations lies within one standard deviation, corresponding to an optimal χ^2 slightly greater than one. Analogous results have been obtained for all other kinds of states here considered. As an example, we report the results of reconstruction based on a Monte Carlo simulated tomography on a squeezed states with $\langle n\rangle = 2$ (one squeezing photon and one signal photon). In Tab. I we report the first few matrix elements compared with the theoretical values. The number probability distribution—the diagonal terms of density matrix $\rho_{n,n}$—is reported in Fig. 3 up to $n = 15$. The maximum index for the matrix elements is limited only by machine memory and precision (at present we compute matrix elements $\rho_{n,m}$ up to $n,m = 31$).

In Fig. 4 a sample of both normalization and mixing is given versus the number of data subensembles, for a highly excited coherent state [less excited states—coherent or not—exhibit a more rapid convergence].

3. – Reconstruction of the Wigner function

The symmetrized Wigner function $W(\alpha,\bar\alpha)$ can be reconstructed from tomographic data using the formula[5]

$$\begin{aligned}\frac{1}{\pi}W(\alpha,\bar\alpha) &= \frac{2}{\pi}\mathrm{Tr}\left[\rho D(2\alpha)\exp\left(i\pi a^\dagger a\right)\right]\\ &= \frac{2}{\pi}\sum_{m,n=0}^{\infty}(-)^n\rho_{n,m}\langle m|D(2\alpha)|n\rangle\ ,\end{aligned}\tag{9}$$

where $D(\alpha)=\exp\left(\bar\alpha a^\dagger-\alpha a\right)$ is the displacement operator. Eq. (9) can be rewritten as Fourier transform

$$W(\alpha,\bar\alpha)=\mathrm{Re}\sum_{d=0}^{\infty}e^{id\phi}\sum_{n=0}^{\infty}\Lambda(n,d;|\alpha|^2)\rho_{n,n+d}\tag{10}$$

where

$$\Lambda(n,d;|\alpha|^2) = (-)^n 2(2-\delta_{d0})|2\alpha|^d \sqrt{\frac{n!}{(n+d)!}} e^{-2|\alpha|^2} L_n^d(|2\alpha|^2) \ , \tag{11}$$

and $L_n^d(x)$ denotes the Laguerre polynomials. We have simulated an optical homodyne tomography (with $F = 27$ scanning phases) performed on a "Schrödinger cat" state (here a superposition of symmetrical coherent states) and then we have reconstructed the Wigner function. Plots of the Wigner function are given in Fig. 5 for a superposition of two coherent states with $\langle n \rangle = 5$ average photons each. As we can see, details and fast oscillations due to quantum interference are well resolved. This is the most improvement of our method with respect to the original smoothed algorithm, because we have no resolution cutoff in phase-space.

4. – Sensitivity

Quantities as phase, field quadrature and photon number could be measured by detecting the density matrix, but also in a direct way by double homodyne,[6] single homodyne, and direct photodetection respectively. Direct measurements give only partial information on the quantum state, and one expects that tomography –providing the maximum available information– should require much more measures in order to achieve the same sensitivity of single-observable detection.
In this section we compare the sensitivity of quantum tomography with those of conventional detection methods [7]. In making such comparison we have to keep in mind that tomography always needs a set of many repeated measurements on the same field: hence, when comparing tomography with single-observable schemes, the same number of repeated measurements must be considered. In a scheme of N repeated measurements of the quantity x, accuracy δx rescales as $\delta x \propto N^{-1/2}$. The proportionality constant generally depends on the kind of detection, and for experimental Gaussian distributions around the average one has that $\delta x = \sqrt{\langle \Delta x^2 \rangle / N}$, $\langle \Delta x^2 \rangle$ being the variance of x. In practice, in order to evaluate δx one can take advantage of the central limit theorem, which assures that the partial average over a block of N_b data is always Gaussian distributed around the global average over many blocks (for large N_b). We compare quantum tomography with double homodyne phase detection, single homodyne quadrature detection, and photon number detection: all sensitivities will be given as a function of the total number of photons $N_T = N\langle n \rangle$ impinged in the apparatus.
The probability distribution of an ideal phase detection is given by[8]

$$P(\varphi) = \frac{1}{2\pi} \sum_{n,m=0}^{\infty} e^{i(m-n)\varphi} \rho_{n,m} \ . \tag{12}$$

The knowledge of the density matrix from tomographic detection allows to evaluate the ideal phase probability (12), that otherwise cannot be directly measured in any known feasible experiment. In a tomographic experiment the reconstructed density matrix leads to an ideal phase distribution which, however, is still sensitive to errors on matrix elements, and thus is affected by fluctuations on the mean value. In other words, even though the ideal phase distribution can be reconstructed from tomographic data, the

variance $\langle \Delta\phi^2 \rangle$ of the distribution does not correspond to the actual sensitivity of the method, and the resulting error $\delta\phi$ on the average phase is much larger than $\sqrt{\langle \Delta\phi^2 \rangle / N}$. As there is no feasible scheme for ideal phase detection (12), we compare tomographic results with those from a double homodyne phase detection.[9] In Fig. 6 the ratio between tomographic and double homodyne phase sensitivities is plotted for various coherent states as a function of the total mean energy impinged into the apparatus. The noise added by tomography is apparent: the ratio between sensitivities is of several decibels. The added noise is almost independent on the total energy impinged in the apparatus, but depends on the mean photon number of the state.
Now we perform the above analysis as regards the field quadrature $\hat{a}_0 = \frac{1}{2}(a + a^\dagger)$ and the photon number. Again quantum tomography adds noise. For the quadrature the ratio of sensitivities depends on the mean photon number of the input state (see in Fig. 6), whereas for number detection such dependence becomes very weak (see Fig. 7).
The asymptotic ratio (for a very large number of repeated experiments) between tomographic and direct single-observable sensitivities is plotted in Fig. 7 versus the number of photons of the input coherent state. In summary, we estimate that, for large numbers of photons and input coherent states, tomography adds more than 10dB of noise in phase detection (with respect to double homodyne), 7dB in photon number detection, and more that 8dB in quadrature detection.

REFERENCES

[1] D. T. Smithey, M. Beck, M. G. Raymer, and A. Faridani, Phys. Rev. Lett. **70**, 1244 (1993).
[2] K. Vogel and H. Risken, Phys. Rev. A **40**, 2847 (1989)
[3] G. M. D'Ariano, C. Macchiavello and M. G. A. Paris, Phys. Rev. A (in press).
[4] I. S. Gradshteyn and I. M. Ryzhik , *Table of integrals, series, and products*(Academic Press, 1980).
[5] K. E. Cahill and R. J. Glauber, Phys. Rev. **177**, 1857 (1969)
[6] Double homodyne detection is actually a density operator detection in the Husimi Q-function representation, however it does not trivially provide all information on the field, because the antinormal form of generic functions of the field operators does not always exist.
[7] G. M. D'Ariano, C. Macchiavello and M. G. A. Paris, Phys. Lett. A (in press).
[8] C. W. Helstrom, *Quantum Detection and Estimation Theory* (Academic Press, New York, 1976)
[9] G. M. D'Ariano and M. G. A. Paris, Phys. Rev. A **49** 3022 (1994)

TABLE I. – *First detected matrix elements of a squeezed state with $\langle n \rangle = 2$ and one squeezing-photon (the matrix is real; the theoretical values are given in parenthesis). The detected values are obtained for 120 experiments with $F = 27$ scanning phases and 120 measurements each.*

	0	1	2	3	4	5
0	0.5279± 0.0013 (0.5275)	0.1538±0.0012 (0.1547)	0.2947±0.0015 (0.2957)	0.1396±0.0016 (0.1393)	0.2006±0.0019 (0.2015)	0.1133±0.0019 (0.1145)
1	0.1538±0.0012 (0.1547)	0.0432±0.0021 (0.0454)	0.0848±0.0014 (0.0867)	0.0418±0.0017 (0.0409)	0.0568±0.0016 (0.0591)	0.0336±0.0015 (0.0336)
2	0.2947±0.0015 (0.2957)	0.0848±0.0014 (0.0867)	0.1657±0.0021 (0.1658)	0.0799±0.0013 (0.0781)	0.1123±0.0016 (0.1130)	0.0666±0.0017 (0.0642)
3	0.1396±0.0016 (0.1393)	0.0418±0.0017 (0.0409)	0.0799±0.0013 (0.0781)	0.0387±0.0020 (0.0368)	0.0519±0.0014 (0.0532)	0.0313±0.0016 (0.0303)
4	0.2006±0.0019 (0.2015)	0.0568±0.0016 (0.0591)	0.1123±0.0016 (0.1130)	0.0519±0.0014 (0.0532)	0.0757±0.0022 (0.0770)	0.0440±0.0015 (0.0437)
5	0.1133±0.0019 (0.1145)	0.0336±0.0015 (0.0336)	0.0666±0.0017 (0.0642)	0.0313±0.0016 (0.0303)	0.0440±0.0015 (0.0437)	0.0271±0.0024 (0.0249)
...	...	...	...	...	...	...

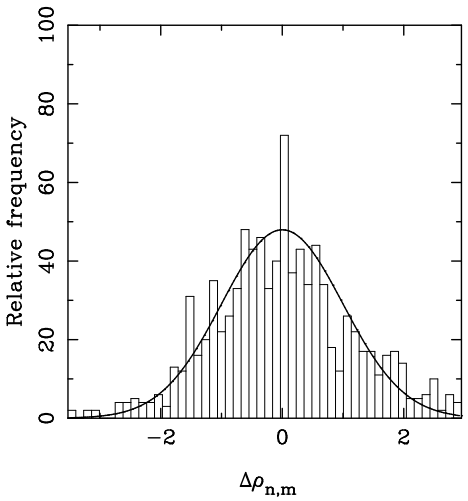

Fig. 2. – Distribution of normalized deviations from the theoretical values $\Delta\rho_{n,m} \equiv (\bar{\rho}_{n,m} - \rho_{n,m})/\varepsilon_{n,m}$ for the first 30×30 matrix elements. The quantum state is a coherent one with $\langle n \rangle = 4$. The histogram pertains 1000 experiments (subensembles of data) with $F = 27$ scanning phases each, and 200 measurements for each phase. A standardized (unit variance) Gaussian curve is superimposed.

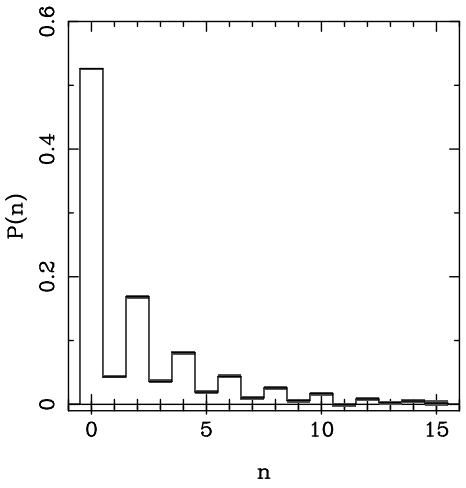

Fig. 3. – Number probability distributions for states of Tab. I ($F = 27$ scanning phases are used; there are 100 experiments and 100 measurements for each phase).

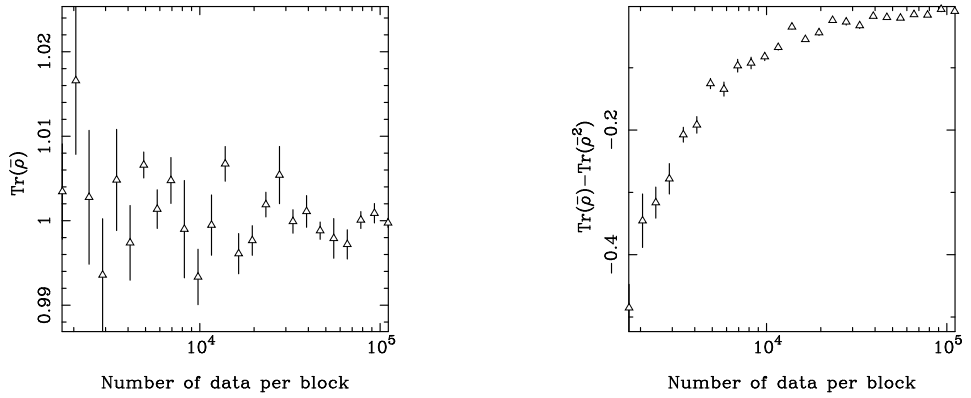

Fig. 4. – Normalization and mixing of the reconstructed density matrix versus the number data for each experiment (subensemble of data) for a coherent state with $\langle n \rangle = 8$. Error bars are estimated on a set of five experiments.

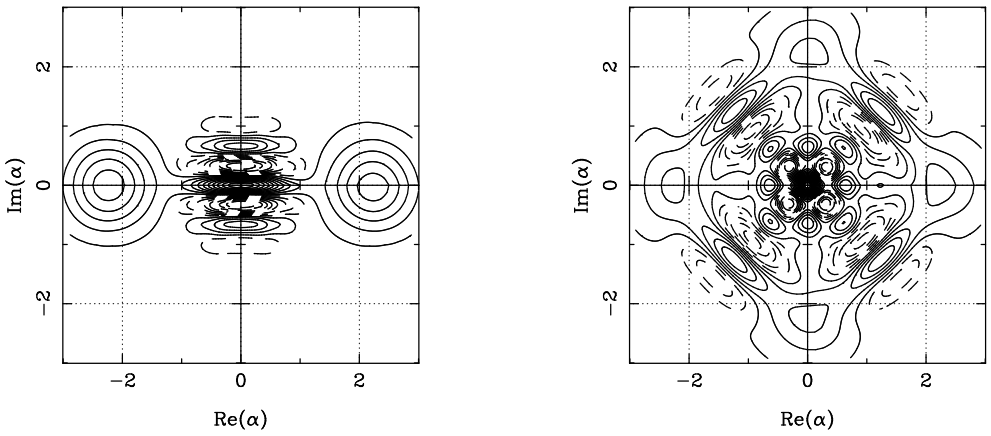

Fig. 5. – Reconstructed Wigner function of quantum superpositions of two and four coherent states with $\langle n \rangle = 5$ each. 1000 experiments of $27 \star 1000$ data each have been used.

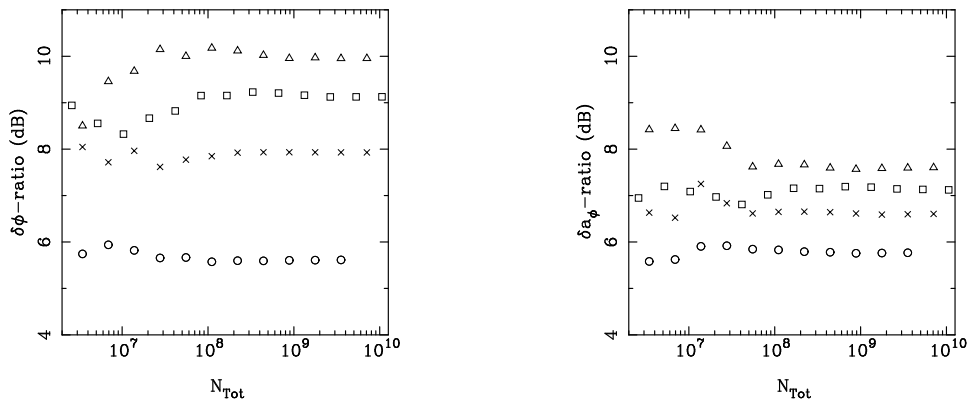

Fig. 6. – Ratio (in dB) between sensitivity from tomographic reconstruction and from direct detection for phase and field quadrature as a function of the total mean number of photons impinged into the apparatus $N_T = N\langle n \rangle$, with N the total number of experiments. Results for different coherent states are reported (circle: $\langle n \rangle = 2$, cross: $\langle n \rangle = 4$, square: $\langle n \rangle = 6$, triangle: $\langle n \rangle = 8$).

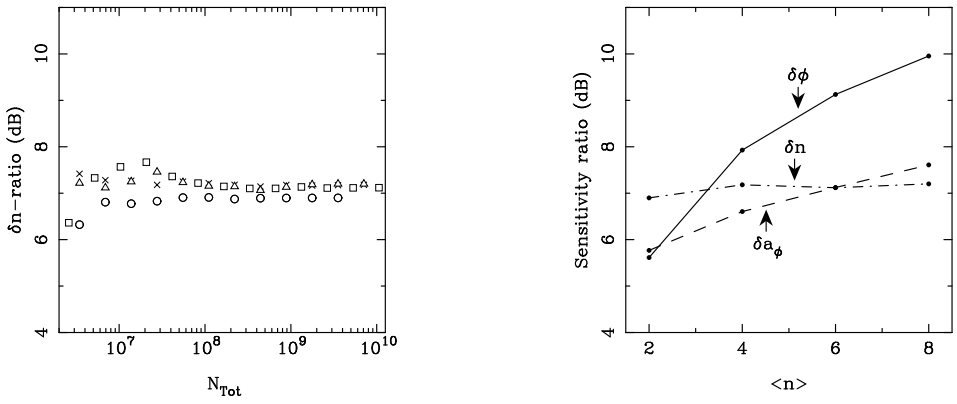

Fig. 7. – Ratio (in dB) as in Fig. 6 for number of photons and asymptotic ratio between tomographic and single-observables sensitivity as a function of the mean photon number of the input coherent states (here $N_{tot} = \langle n \rangle * 65536 * 1000 * 27$).